Supporting Information for

Low-coordinate Bis(imidazolin-2-iminato) Dysprosium(III) Single-Molecule Magnets

Rong Sun,[§a] Chen Wang,[§a] Bing-Wu Wang,*[a] Zhe-Ming Wang,[a] Yao-Feng Chen,[b] Matthias Tamm,[c] and Song Gao*[a,b]

[a]Beijing National Laboratory for Molecular Sciences, State Key Laboratory of Rare Earth Materials Chemistry and Applications, College of Chemistry and Molecular Engineering, Peking University, Beijing 100871, *P. R. China.* E-mail: wangbw@pku.edu.cn; gaosong@pku.edu.cn

[b]Spin-X Institute, School of Chemistry and Chemical Engineering, State Key Laboratory of Luminescent Materials and Devices, Guangdong-Hong Kong-Macao Joint Laboratory of Optoelectronic and Magnetic Functional Materials, South China University of Technology, Guangzhou 510641, *P. R. China.*

[c]Institut für Anorganische und Analytische Chemie, Technische Universität Carolo-Wilhelmina, Hagenring 30, 38106 Braunschweig, Germany

[§]These authors contributed equally to this work.

1. Experimental Details

General: All operations were carried out under an atmosphere of argon using Schlenk techniques or in an argon filled glovebox. Toluene and hexane were collected from a Vigor YJC-5 Solvent Purification System under argon, transferred to the glove box without exposure to air, and stored in glovebox. Tetrahydrofuran (THF) were dried over $LiAlH_4$, transferred under vacuum, and stored in the glovebox. Anhydrous DyI_3 was commercially available and used without further purification. Benzyl dysprosium(III) complex ($[DyBn_3(THF)_3]$)[1], triethylammonium tetraphenylborate ($[HNEt_3][BPh_4]$)[2] and 1,3-bis(2,6-diisopropylphenyl) imidazolin-2-imine ($Im^{Dipp}NH$)[3] were synthesized according to literature procedures.

Synthesis of $[Dy(Im^{Dipp}N)_2(Bn)(THF)]$ (1): $[DyBn_3(THF)_3]$ (196 mg, 0.30 mmol) and $Im^{Dipp}NH$ (242 mg, 0.60 mmol) were separately dissolved in cooled toluene, and then the $Im^{Dipp}NH$ solution was dropwise added to the $[DyBn_3(THF)_3]$ solution with rapid stirring. The reaction mixture was stirred at room temperature for 30 minutes and then filtered. The yellow filtrate was concentrated to 2 mL at room temperature under reduced pressure. After standing at room temperature overnight, yellow crystals of **1** (203 mg, 0.18 mmol, 60% yield) were obtained. Anal. Calcd. for $C_{65}H_{87}DyN_6O$: C, 69.03; H, 7.75; N, 7.43. Found C, 69.58; H, 7.54; N, 7.32.

Synthesis of $[Dy(Im^{Dipp}N)_2(BPh_4)]$ (2): Crystals of **1** (339 mg, 0.30 mmol) was dissolved in toluene, and then treated with $[HNEt_3][BPh_4]$ (126 mg, 0.30 mmol). The reaction mixture was stirred at room temperature for 30 minutes and then filtered. The yellow filtrate was concentrated to 2 mL at room temperature under reduced pressure. After standing at room temperature overnight, yellow crystals of **2** (289 mg, 0.21 mmol, 70% yield) were obtained. Anal. Calcd. for $C_{78}H_{92}BDyN_6(C_7H_8)$: C, 74.03; H, 7.31; N, 6.09. Found C,74.16; H, 7.46; N, 5.75.

2. X-ray Crystallography.

The single crystal of **1** and **2** covered in grease was mounted under nitrogen atmosphere on a glass fiber. The diffraction data were collected at 180 K using a Rigaku Oxford diffractometer equipped with a CCD collector using Mo Kα radiation (λ = 0.71073 Å). Using Olex2, the structures were solved with the ShelXT structure solution program using Direct Methods or Patterson Method and refined with the ShelXL refinement package using Least Squares minimisation. Hydrogen atoms were placed at calculated positions and were included in the structure calculation. Crystallographic data and refinement for **1** and **2** are listed in Table S1.

Table S1. Crystallographic Data and Refinement parameters of **1** and **2**.

	1	**2**
Formula	$C_{65}H_{87}DyN_6O$	$C_{78}H_{92}BDyN_6 \cdot (C_7H_8)$
Formula Weight	1130.9	1379.1
Color	yellow	yellow
Crystal System	triclinic	orthorhombic
Space Group	$P\bar{1}$	*Fdd2*
a, Å	11.64130(10)	64.3659(5)
b, Å	12.2918(2)	36.0437(4)
c, Å	23.6245(3)	14.09180(10)
α, deg	97.9620(10)	90
β, deg	96.6210(10)	90
γ, deg	114.1740(10)	90
V, Å^3	2998.44(7)	32692.8(5)
Z	2	16
*D*calcd, (g/cm^3)	1.253	0.345
F(000)	1186.0	3553.0
T(K)	180.00(10)	180.00(10)
θ range, deg	2.031, 30.219	2.209, 29.520
No. of refns collected	96666	140728
No. of unique refns	16182	21196
No. of obsd refns ($I > 2\sigma(I)$)	14971	16327
No. of params	694	791
Final *R*, *wR*2 ($I > 2\sigma(I)$)	0.0432, 0.1269	0.0404, 0.0810
Goodness-of-fit on F^2	1.360	0.972
$\Delta\rho_{max, min}$, eÅ^{-3}	2.218, -2.195	0.195, -0.438

Table S2. Selected bond distances [Å] and angles [deg] of **1**.

	1
N−Dy−N (deg)	123.21(13)
N−Dy−C (deg)	104.78(14), 110.65(15)
N−Dy−O (deg)	97.95(12), 102.23(12)
Dy−N (Å)	2.132(3), 2.145(4)
Dy−C (Å)	2.464(4)
Dy−O (Å)	2.339(3)

Table S3. Selected bond distances [Å] and angles [deg] of **2**.

	2
N−Dy−N (deg)	118.28(15)
N−Dy−C (deg)	80.81(14), 94.25(16), 91.21(14), 118.60(14), 93.13(13), 117.88(14), 120.43(13), 137.32(14), 134.63(14), 121.20(16), 116.09(16), 88.57(16), 137.67(14), 117.82(14), 129.91(14), 82.13(14), 113.24(13), 85.86(15), 91.11(14), 73.85(15),
N−Dy−$Ph_{centroid}$* (deg)	106.16, 109.93, 101.99, 109.10
Dy−N (Å)	2.157(4), 2.120(4)
Dy−C (Å)	2.855(4), 2.926(5), 2.880(4), 2.964(5), 2.888(4), 2.887(5), 2.872(5), 2.915(5), 2.911(4), 2.911(5)
Dy−$Ph_{centroid}$* (Å)	2.577, 2.547

*$Ph_{centroid}$ represents the center of the coordinated phenyl.

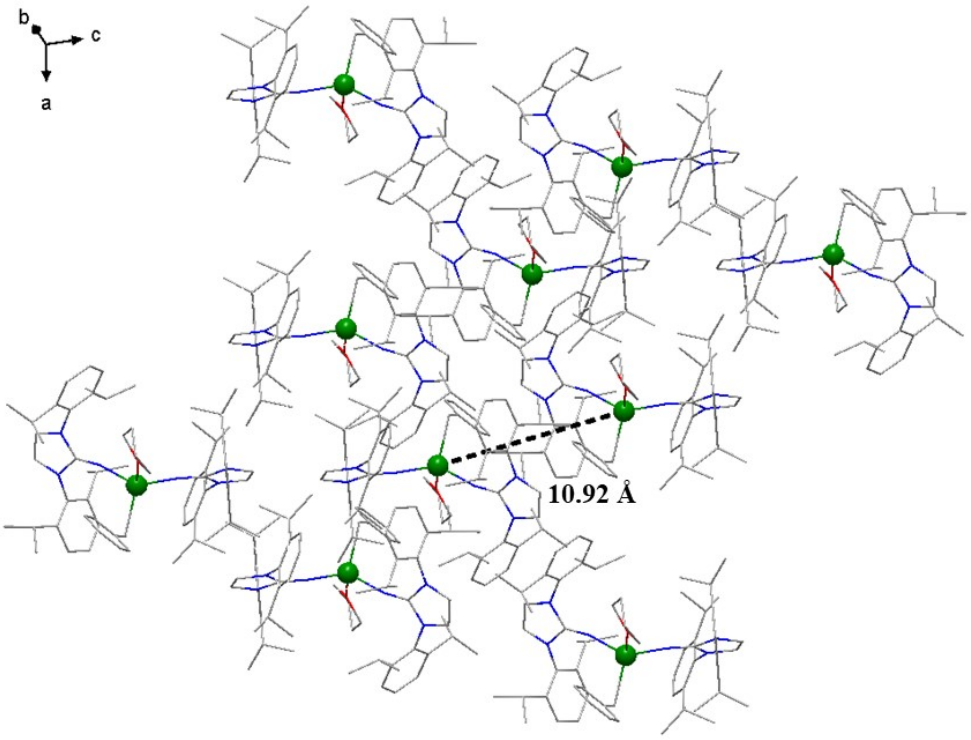

Figure S1. The molecular packing in **1**. Color codes: Dy, green; N, blue; O, red; C, grey; For clarity, hydrogen atoms are omitted.

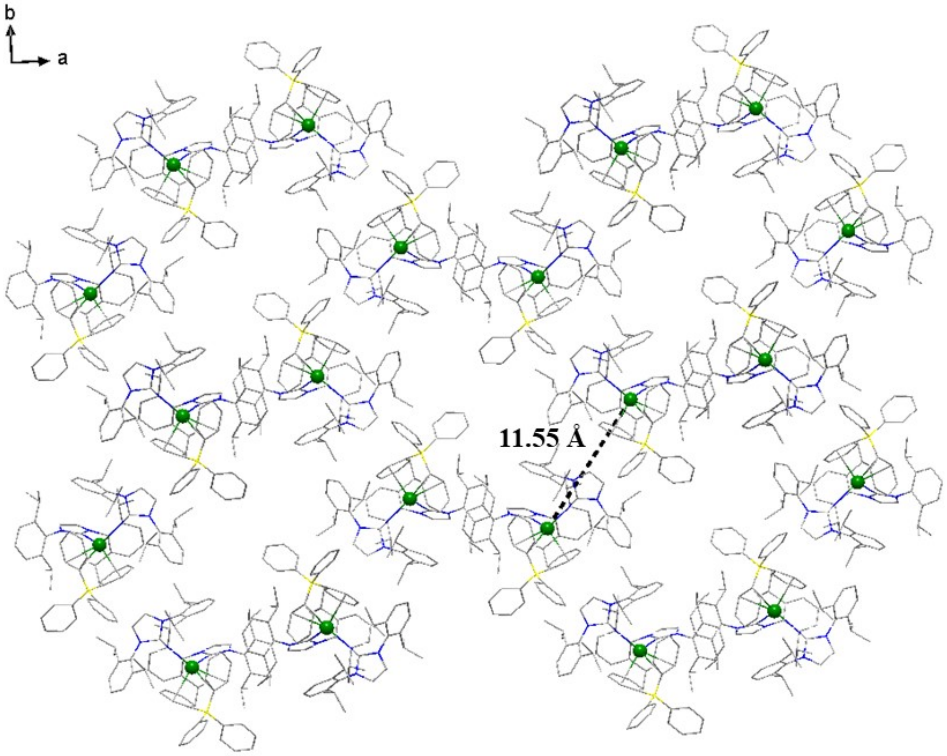

Figure S2. The molecular packing in **2**. Color codes: Dy, green; N, blue; B, yellow; C, grey; For clarity, hydrogen atoms are omitted.

3. Magnetic Properties

The samples were packed in capsules with N-grease and parafilm covered to protect them from air and water. DC mode was adopted for the measurements of susceptibility and magnetization, while VSM mode was selected for hysteresis and ZFC-FC measurements on Quantum Design MPMS3 magnetometer. Ac magnetic measurements were performed both on Quantum Design PPMS magnetometer (100 ~ 10000 Hz). The background of sample holders (capsule, parafilm and N-grease) and Pascal correction were considered when the diamagnetic correction was carried on the data.

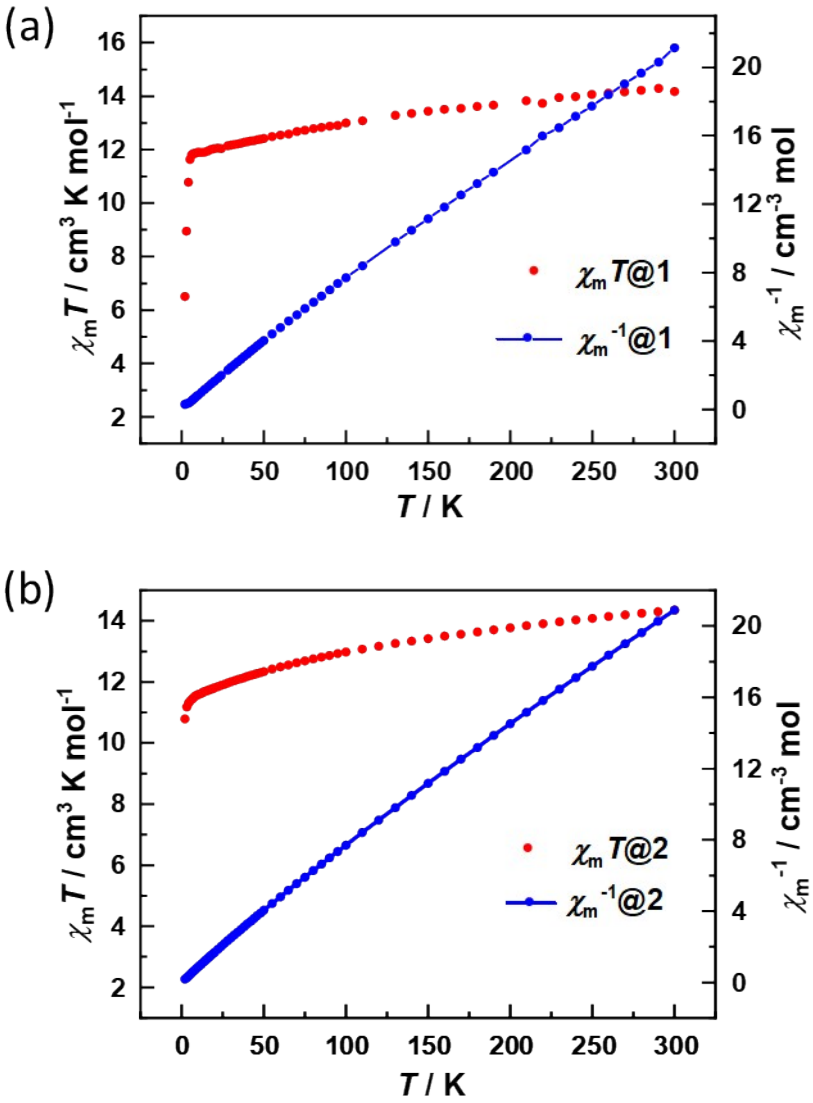

Figure S3. Temperature dependence of $\chi_m T$ and χ_m^{-1} for **1** (a) and **2** (b) at 1 kOe dc field.

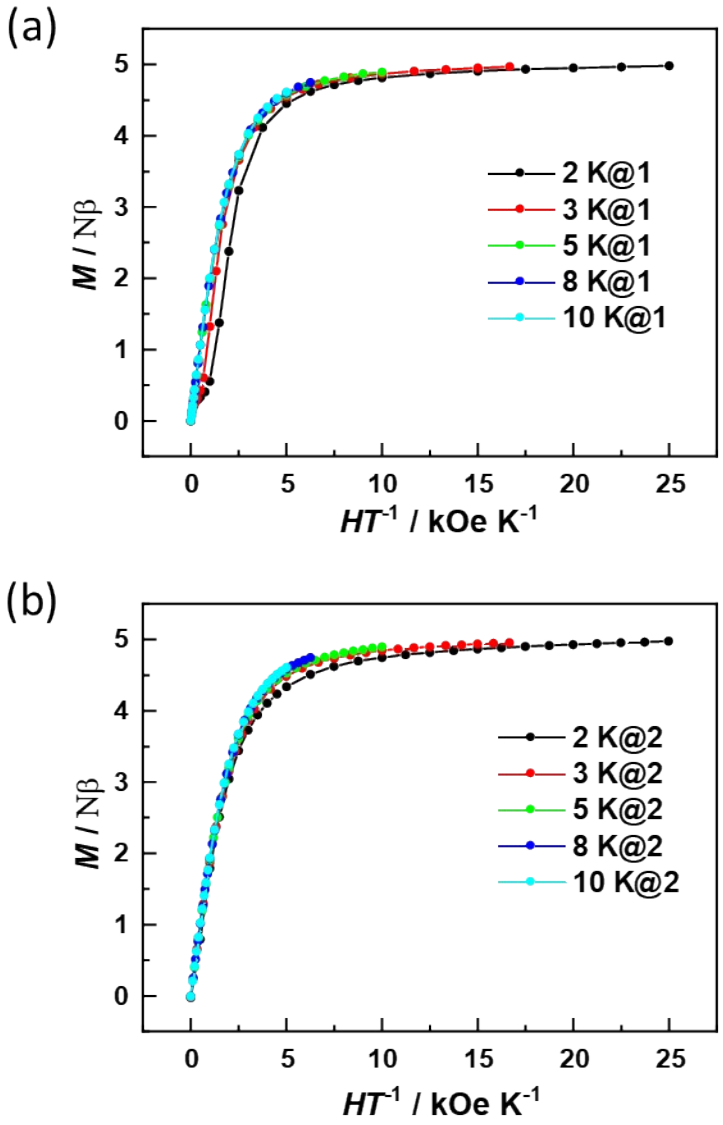

Figure S4. Plots of magnetization *M* versus *H*/*T* at the temperature of 2 K, 3 K, 5 K, 8 K and 10 K for **1** (a) and **2** (b).

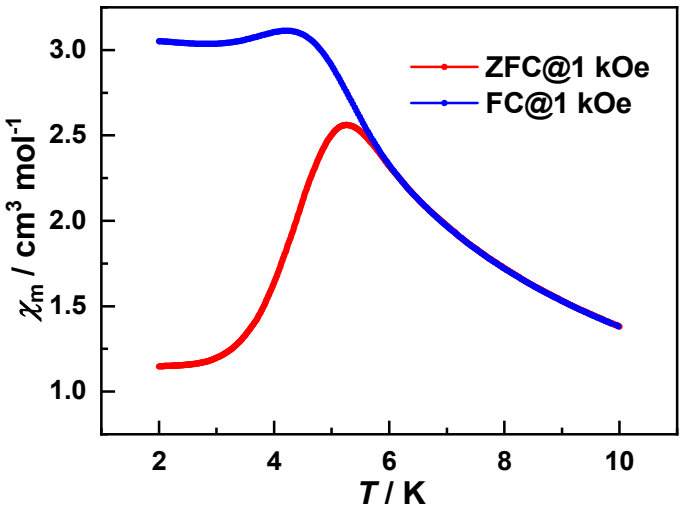

Figure S5. Zero-field-cooled (ZFC) magnetization and field-cooled (FC) magnetization of **1** under 1 kOe at sweep rate of 3 K min^{-1} with the lines are guides for the eyes.

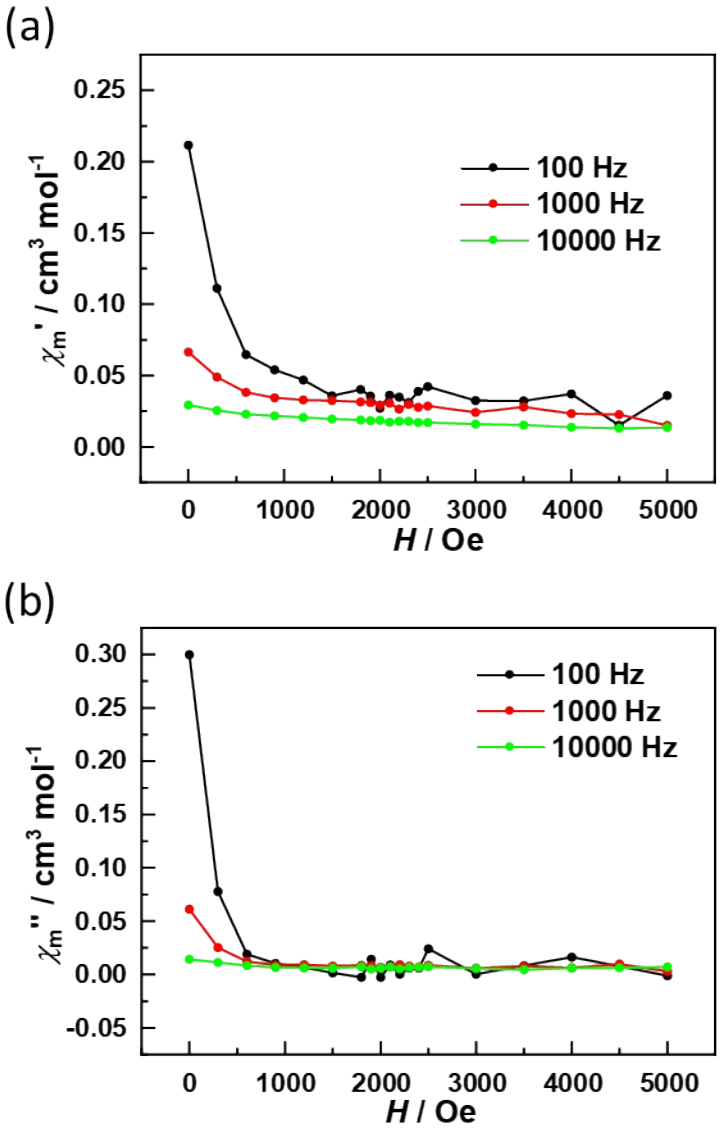

Figure S6. Plots of field dependent in-phase (χ_m') and out-of-phase (χ_m'') component of ac susceptibility of **1** at 2 K.

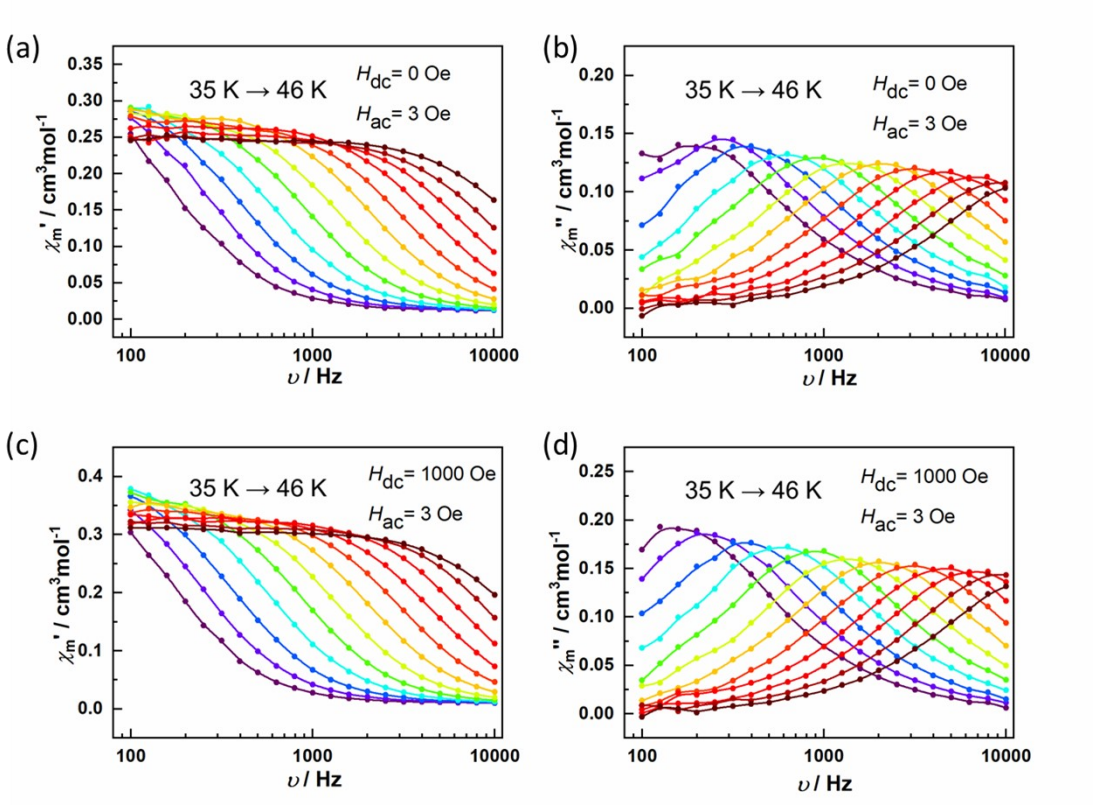

Figure S7. Plots of frequency dependent in-phase (χ_m') and out-of-phase (χ_m'') component of ac susceptibility of **1** at zero field and 1000 Oe dc field.

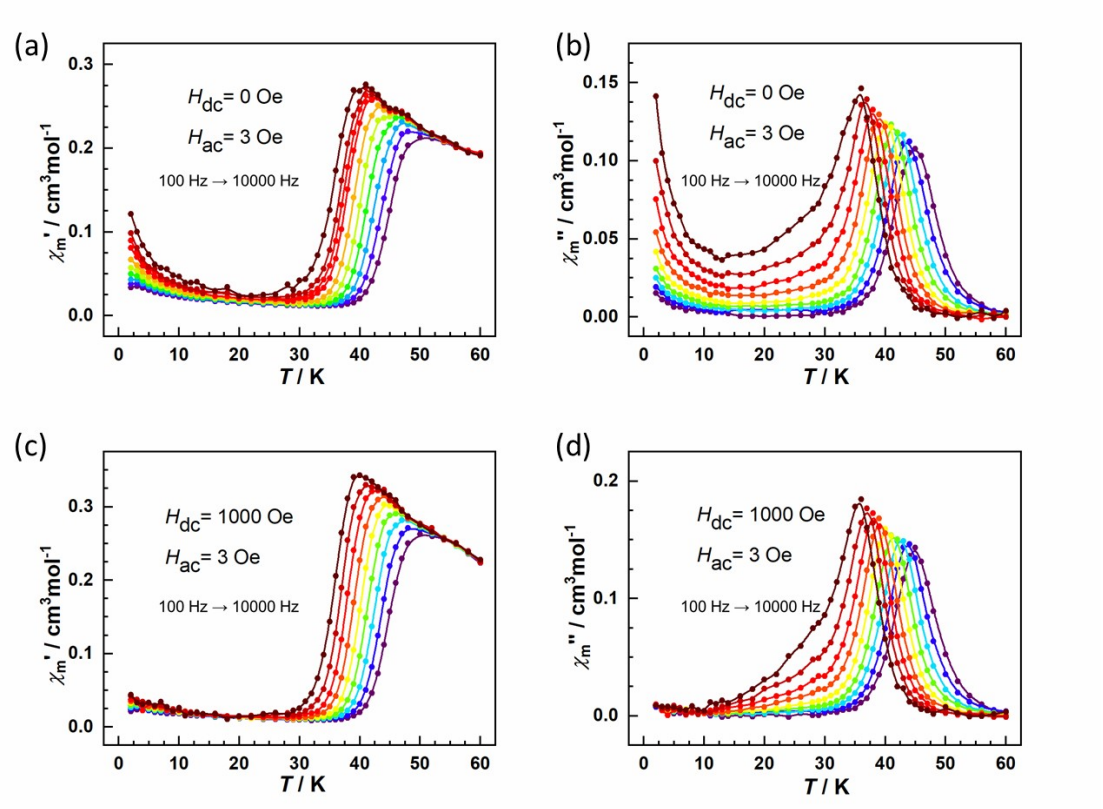

Figure S8. Plots of temperature dependent in-phase (χ_m') and out-of-phase (χ_m'') component of ac susceptibility of **1** under zero field and 1000 Oe dc field.

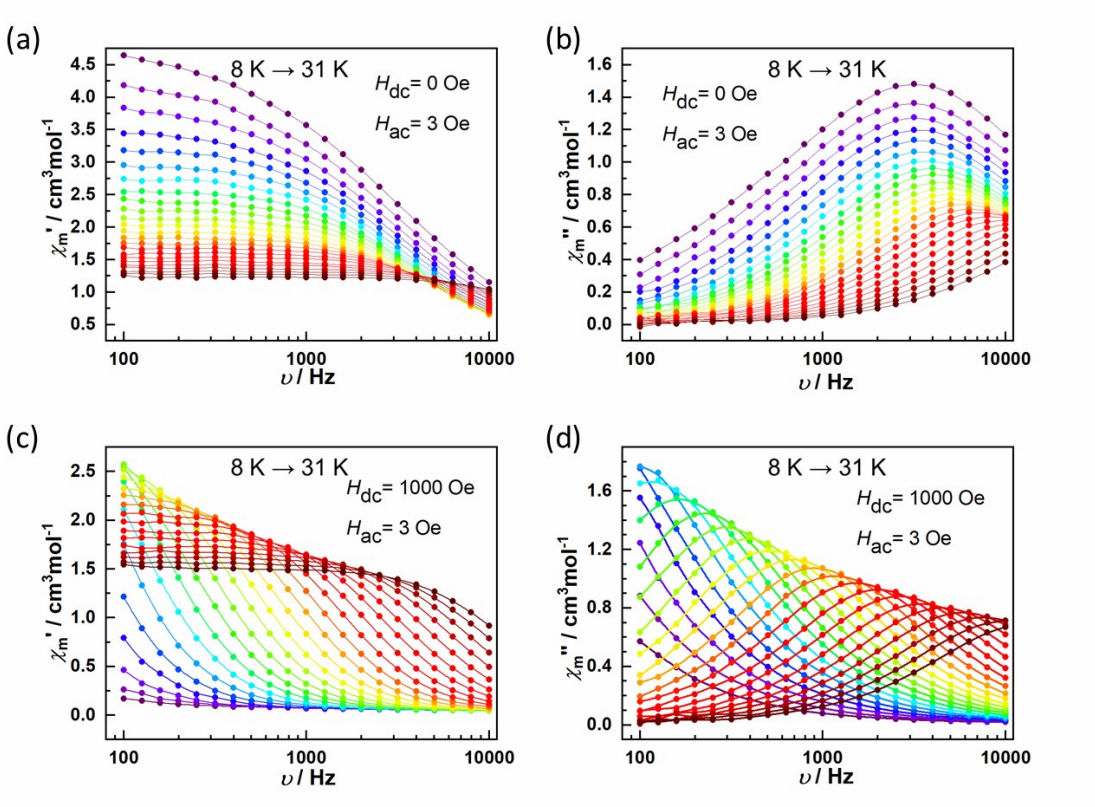

Figure S9. Plots of frequency dependent in-phase (χ_m') and out-of-phase (χ_m'') component of ac susceptibility of **2** at zero field and 1000 Oe dc field.

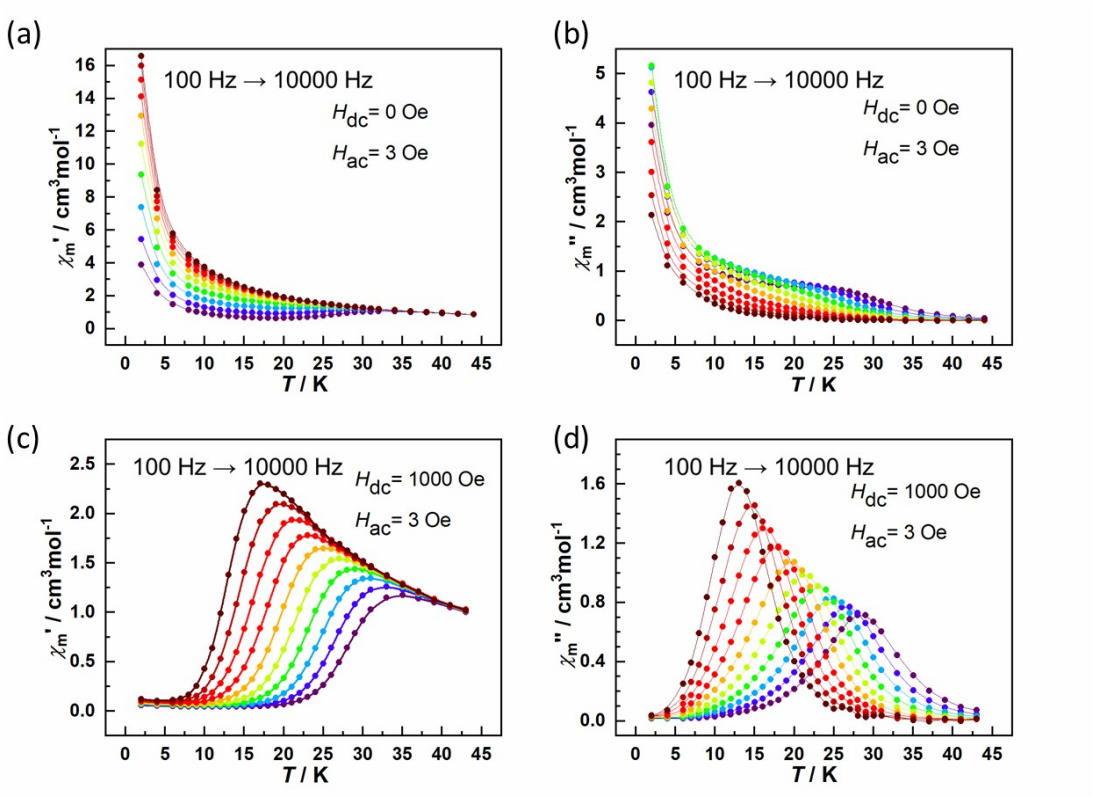

Figure S10. Plots of temperature dependent in-phase (χ_m') and out-of-phase (χ_m'') component of ac susceptibility of **2** under zero field and 1000 Oe dc field.

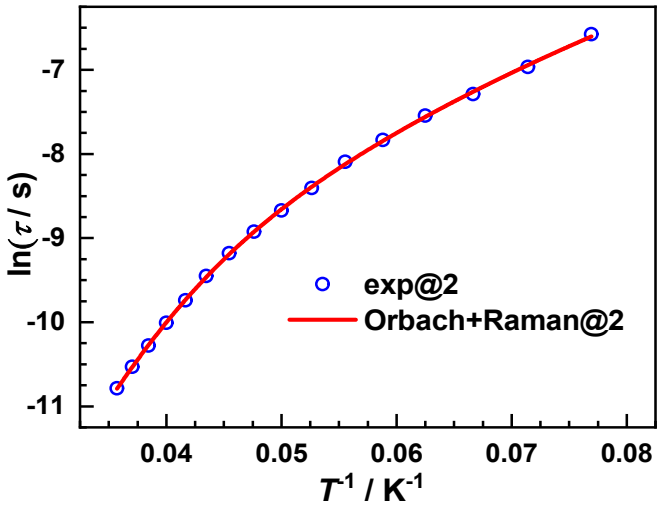

Figure S11. The lnτ versus T^{-1} plots at 1000 Oe dc field for **2**. The solid lines represent the fitting results.

4. Theoretical Analysis

Ab initio calculations were performed with MOLCAS 8.1 program[4]. For complex **1** and **2**, the calculation fragments were all built based on the crystal structures. The basis sets for all atoms are atomic natural orbitals from the MOLCAS ANO-RCC library[5-6]: ANO-RCC-VTZP for Dy(III) ions; VTZ for close N/O/C; VDZ for distant atoms. The calculations employed the second order Douglas-Kroll-Hess Hamiltonian, where scalar relativistic contractions were considered in the basis sets and the spin-orbit couplings were handled in the restricted active space state interaction (RASSI-SO) procedure. We have mixed the maximum number of spin-free states which was possible with our hardware (all from 21 sextets, 128 from 224 quadruplets, 130 from 490 doublets for the Dy(III) fragment). Active electrons in seven active spaces include all f electrons (CAS (9, 7)) of Dy (III) in the CASSCF calculation. For model fragment $[Dy(N^{RR'})_2]^+$ and $[Dy(Im^{Dipp}N)_2]^+$, the basis sets are: ANO-RCC-VTZP for Dy(III) ions; VTZ for close N/Cl; VDZ for distant atoms. The predicted U_{eff} versus the angles of N−Dy−N for $[Dy(Im^{Dipp}N)_2]^+$ fragment was fitted using quadratic function(Table S8).

Model molecule $[Dy(Im^{Dipp}N)_2(THF)_4]^+$ was constructed based on the crystal structure of $[Dy\{OB(NArCH)_2\}_2(THF)_4]^+$ by replacing B–O with C–N and optimized based on Density Function Theory (DFT) employing the B3LYP functional[7-8] in Gaussian 09[9]. During the optimization, the dysprosium(III), the coordinated O and N were frozen. Then *ab initio* calculation at the same level of theory was conducted. The basis sets are: ANO-RCC-VTZP for Dy(III) ions; VTZ for close N/O; VDZ for distant atoms. Model molecule $[Dy(Im^{Dipp}N)_2(THF)_3]^+$ was constructed by removing one THF molecule of $[Dy(Im^{Dipp}N)_2(THF)_4]^+$, and adjusting the N–Dy–N angle to be 180°, O–Dy–O angle to be 90°. Then *ab initio* calculation at the same level of theory was also conducted.

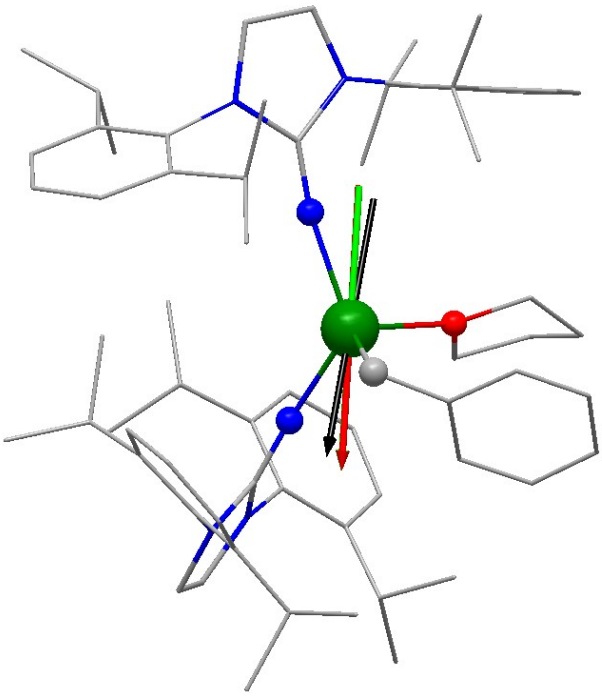

Figure S12. Orientations of easy axis of the KDs on Dy(III) for **1**. The green arrow represents the ground KDs, the red stands for the first excited KDs and the black corresponds to the second excited KDs. Color codes: Dy, green; N, blue; O, red; C, grey; For clarity, hydrogen atoms are omitted.

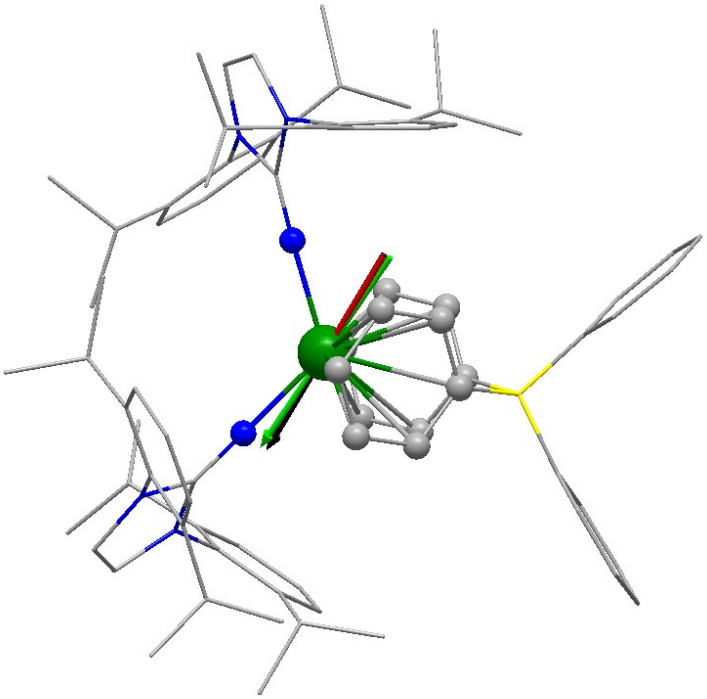

Figure S13. Orientations of easy axis of the KDs on Dy(III) for **2**. The green arrow represents the ground KDs, the red stands for the first excited KDs and the black corresponds to the second excited KDs. Color codes: Dy, green; N, blue; O, red; C, grey; B: yellow. For clarity, hydrogen atoms are omitted.

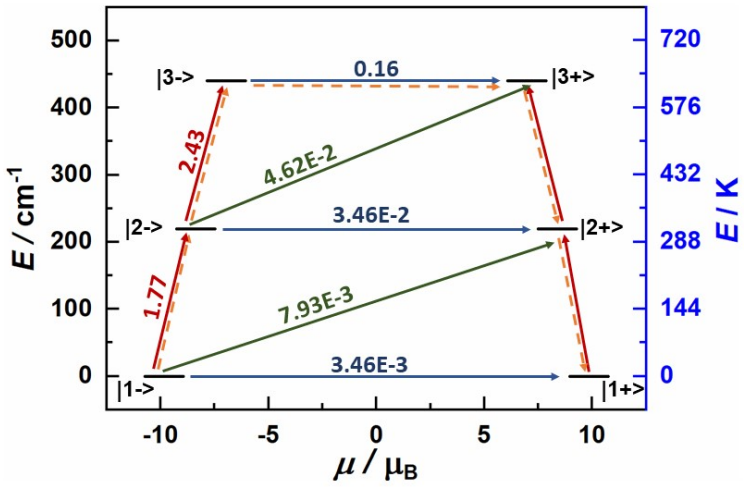

Figure S14. The magnetic blocking barriers for **2**. The thick black lines represent the KDs as a function of their magnetic moment along the magnetic axis. The blue lines within KDs correspond to quantum tunneling of magnetization (QTM), and the numbers at each arrow represent the mean absolute value of the corresponding matrix element of transition magnetic moment. The orange dashed arrows show the deduced relaxation pathway.

Table S4. Calculated energy levels and g (g_x, g_y, g_z) tensors of the lowest Kramers doublets (KDs) of individual Dy(III) fragment for **1** and **2**.

KDs	**1**			**2**		
	E / cm^{-1}	E / K	g	E / cm^{-1}	E / K	g
1	0.0	0.0	0.002 0.002 19.817	0.0	0.0	0.008 0.013 19.685
2	234.8	337.6	0.043 0.058 17.021	219.4	315.6	0.093 0.107 16.775
3	362.2	520.8	1.459 2.620 14.296	440.3	633.2	0.418 0.507 13.959
4	416.1	598.4	1.370 4.229 9.634	636.7	915.5	1.679 2.332 11.100
5	497.6	715.5	4.527 5.165 8.900	790.8	1137.2	0.171 3.507 8.647
6	592.1	851.5	0.810 1.163 13.987	885.4	1273.2	3.026 5.601 8.464
7	725.5	1043.3	0.034 0.059 17.296	948.6	1364.1	1.461 3.617 15.900
8	990.0	1423.6	0.001 0.001 19.838	1062.4	1527.7	0.039 0.139 19.595

Table S5. Wave functions with definite projection of the total moment $|m_J>$ for of the lowest Kramers doublets (KDs) of individual Dy(III) fragment for **1** and **2**.

	E / cm^{-1}	wave functions
1	0.0	99.6%|±15/2>
	234.8	93.4%|±13/2>+2.7%|±11/2>+3.0%|±9/2>
	362.2	38.9%|±11/2>+9.3%|±9/2>+16.1%|±7/2>+10.4%|±5/2>+10.9%|±3/2>+9.9%|±1/2>+4.4%|±13/2>
2	0.0	98.1%|±15/2>
	219.4	94.6%|±13/2>+4.4%|±9/2>
	440.3	88.2%|±11/2>+7.4%|±7/2>+1.9%|±15/2>

Table S6. Calculated energy levels and g (g_x, g_y, g_z) tensors of the lowest Kramers doublets (KDs) of individual Dy(III) fragment for artificial structure **[Dy(Im^{Dipp}N)$_2$]$^+$** with different N−Dy−N angles.

N−Dy−N / deg	**123.2**		**133.2**		**143.2**		**153.2**		**163.2**		**173.2**	
KDs	E / cm^{-1}	g	E / cm^{-1}	g	E / cm^{-1}	g	E / cm^{-1}	g	E / cm^{-1}	g	E / cm^{-1}	g
		0.000		0.000		0.000		0.000		0.000		0.000
1	0.0	0.000	0.0	0.000	0.0	0.000	0.0	0.000	0.0	0.000	0.0	0.000
		19.771		19.803		19.828		19.851		19.874		19.895
		0.000		0.000		0.000		0.000		0.000		0.000
2	494.7	0.000	589.0	0.000	669.2	0.000	732.5	0.000	776.9	0.000	800.1	0.000
		16.876		16.871		16.851		16.833		16.825		16.830
		0.000		0.000		0.000		0.000		0.000		0.000
3	914.4	0.000	1099.2	0.000	1262.4	0.000	1394.8	0.000	1488.4	0.000	1537.2	0.000
		14.089		14.076		14.023		13.964		13.921		13.907
		0.014		0.001		0.002		0.002		0.003		0.005
4	1249.3	0.016	1501.4	0.001	1731.7	0.002	1923.0	0.002	2060.3	0.003	2131.8	0.005
		11.397		11.427		11.383		11.308		11.241		11.212
		0.376		0.101		0.093		0.137		0.312		0.445
5	1496.5	0.409	1782.4	0.111	2046.3	0.099	2267.3	0.152	2426.6	0.365	2509.7	0.536
		8.752		8.887		8.897		8.804		8.667		8.574
		3.735		2.038		1.855		3.564		4.228		4.017
6	1660.2	3.824	1953.7	2.121	2219.4	1.935	2437.5	3.741	2591.5	5.250	2671.7	5.908
		5.826		6.289		6.431		6.473		7.666		8.413
		2.289		9.205		9.556		1.819		1.057		0.708
7	1759.7	5.511	2044.0	6.332	2297.7	7.213	2508.3	5.990	2665.2	3.529	2749.2	2.408
		11.653		2.844		2.603		11.806		13.614		14.252
		0.289		0.539		0.383		0.174		0.153		0.139
8	1853.6	0.854	2106.9	1.982	2356.7	1.277	2577.2	0.466	2739.0	0.332	2823.2	0.264
		18.639		17.673		18.095		18.895		19.217		19.328

Table S7. Calculated energy levels and g (g_x, g_y, g_z) tensors of the lowest Kramers doublets (KDs) of individual Dy(III) fragment for artificial structure **[Dy(Im^{Dipp}N)$_2$]$^+$** with linear N−Dy−N angle.

KDs	E / cm^{-1}	E / K	g_x	g_y	g_z
1	0.0	0.0	0.000	0.000	19.909
2	801.6	1152.8	0.000	0.000	16.836
3	1534.8	2207.0	0.000	0.000	13.907
4	2123.0	3052.8	0.013	0.014	11.171
5	2497.2	3591.0	0.835	1.055	8.307
6	2660.0	3825.0	8.477	6.905	3.770
7	2757.9	3965.8	0.333	1.068	15.005
8	2848.7	4096.4	0.058	0.087	19.466

Table S8. Calculated energy levels and g (g_x, g_y, g_z) tensors of the lowest Kramers doublets (KDs) of individual Dy(III) fragment for artificial bis(amido) structure **[Dy($N^{RR'}$)$_2$]$^+$**.

KDs	E / cm^{-1}	E / K	g_x	g_y	g_z
1	0.0	0.0	0.000	0.000	19.908
2	764.5	1099.3	0.000	0.000	16.870
3	1516.7	2181.0	0.000	0.000	13.914
4	2146.1	3086.1	0.000	0.000	11.236
5	2534.8	3645.0	0.140	0.152	8.828
6	2662.2	3828.2	2.043	5.168	12.237
7	2683.6	3859.0	0.949	5.532	11.346
8	2698.9	3881.0	0.031	2.356	16.408

Table S9. The fitting of the predicted U_{eff} versus the angles of N−Dy−N for $[Dy(Im^{Dipp}N)_2]^+$ fragment using a Parabola model.

Equation	$y = A + B * X + C * X^2$
A	-12836.1 ± 2623.6
B	187.4 ± 34.9
C	-0.53 ± 0.08
R^2	0.981

Table S10. Calculated energy levels and g (g_x, g_y, g_z) tensors of the lowest Kramers doublets (KDs) of individual Dy(III) fragment for artificial structure **[Dy(Im^{Dipp}N)$_2$(THF)$_4$]$^+$**.

KDs	E / cm^{-1}	E / K	g_x	g_y	g_z
1	0.0	0.0	0.001	0.001	19.851
2	543.2	781.1	0.042	0.056	16.763
3	945.3	1359.4	0.936	4.526	12.969
4	1143.9	1644.9	4.542	5.458	10.038
5	1290.3	1855.4	0.395	1.807	10.998
6	1416.2	2036.6	0.239	0.826	17.142
7	1449.3	2084.0	0.381	0.683	17.561
8	1561.0	2244.6	0.175	0.230	18.797

Table S11. Calculated energy levels and g (g_x, g_y, g_z) tensors of the lowest Kramers doublets (KDs) of individual Dy(III) fragment for artificial structure **[Dy(Im^{Dipp}N)$_2$(THF)$_3$]$^+$**.

KDs	E / cm^{-1}	E / K	g_x	g_y	g_z
1	0.0	0.0	0.000	0.000	19.887
2	604.3	869.0	0.008	0.010	16.909
3	1111.0	1597.6	0.153	0.184	13.974
4	1456.0	2093.7	2.160	3.049	10.286
5	1603.9	2306.4	3.260	5.192	11.488
6	1681.9	2418.6	0.811	1.464	12.734
7	1785.8	2567.9	0.031	0.259	17.728
8	1879.2	2702.2	0.037	0.079	19.315

5. References

1. A. J. Wooles, D. P. Mills, W. Lewis, A. J. Blake and S. T. Liddle, Lanthanide tri-benzyl complexes: structural variations and useful precursors to phosphorus-stabilised lanthanide carbenes, *Dalton Trans*., 2010, **39**, 500–510.
2. N. M. Kuuloja, T. M. Kylmälä, J. E. Tois, R. E. Sjöholm and R. G. Franzén, Lanthanide tri benzyl complexes: structural variations and useful precursors to phosphorus-stabilised lanthanide carbenes, *Synth. Commun.*, 2011, **41**, 1052–1063.
3. M. Tamm, D. Petrovic, S. Randoll, S. Beer, T. Bannenberg, P. G. Jones and J. Grunenberg, Structural and theoretical investigation of 2-iminoimidazolines–carbene analogues of iminophosphoranes, *Org. Biomol. Chem.*, 2007, **5**, 523–530.
4. F. Aquilante, J. Autschbach, R. K. Carlson, L. F. Chibotaru, M. G. Delcey, L. De Vico, I. Fdez Galván, N. Ferré, L. M. Frutos, L. Gagliardi, M. Garavelli, A. Giussani, C. E. Hoyer, G. Li Manni, H. Lischka, D.-X Ma, P.-Å. Malmqvist, T. Müller, A. Nenov, M. Olivucci, T. B. Pedersen, B.-D. Peng, F. Plasser, B. Pritchard, M. Reiher, I. Rivalta, I. Schapiro, J. Segarra-Martí, M. Stenrup, D. G. Truhlar, L. Ungur, A. Valentini, S. Vancoillie, V. Veryazov, V. P. Vysotskiy, O. Weingart, F. Zapata and R. Lindh, MOLCAS 8: New Capabilities for Multiconfigurational Quantum Chemical Calculations across the Periodic Table, *J. Comput. Chem.*, 2016, **37**, 506–541.
5. B. O. Roos, R. Lindh, P.-Å. Malmqvist, V. Veryazov and P.-O. Widmark, Main Group Atoms and Dimers Studied with a New Relativistic ANO Basis Set, *J. Phys. Chem. A*, 2004, **108**, 2851–2858.
6. B. O. Roos, R. Lindh, P.-Å. Malmqvist, V. Veryazov and P.-O. Widmark, New relativistic ANO basis sets for actinide atoms, *Chem. Phys. Lett.*, 2005, **409**, 295–299.
7. C. Lee, W.-T. Yang and R. G. Parr, Development of the Colic-Salvetti correlation-energy formula into a functional of the electron density, *Phys. Rev. B*, 1988, **37**, 785–789.
8. A. D. Becke, Density-functional thermochemistry. III. The role of exact exchange, *J. Chem. Phys.*, 1993, **98**, 5648–5652.
9. M. J. Frisch, G. W. Trucks, H. B. Schlegel, G. E. Scuseria, M. A. Robb, J. R. Cheeseman, G. Scalmani, V. Barone, B. Mennucci and G. A. Petersson, Gaussian 09 Rev. A.02, Wallingford, CT, 2009.